ACS SENSORS

pubs.acs.org/acssensors Article

Electrical Detection Assay Based on Programmable Nucleic Acid Probe for Efficient Single-Nucleotide Polymorphism Identification

Yun Zhang, Bo Chen, Duo Chen, Yiming Wang, Qingqing Lu, Jie Tan, Long Chen, Liping Zhou, Weihong Tan, Yanbing Yang,* and Quan Yuan*

Cite This: *ACS Sens.* 2023, 8, 2096−2104 Read Online

ACCESS | Metrics & More | Article Recommendations | Supporting Information

ABSTRACT: The large-scale pandemic and fast evolution of severe acute respiratory syndrome coronavirus 2 (SARS-CoV-2) variants have triggered an urgent need for an efficient and sensitive on-site nucleic acid testing method with single-nucleotide polymorphism (SNP) identification capability. Here, we report a multiplexed electrical detection assay based on a paperclip-shaped nucleic acid probe (PNprobe) functionalized field-effect transistor (FET) biosensor for highly sensitive and specific detection and discrimination of SARS-CoV-2 variants. The three-stem structure of the PNprobe significantly amplifies the thermodynamic stability difference between variant RNAs that differ in a single-nucleotide mutation. With the assistance of combinatorial FET detection channels, the assay realizes simultaneously the detection and identification of key mutations of seven SARS-CoV-2 variants, including nucleotide substitutions and deletions at single-nucleotide resolution within 15 min. For 70 simulated throat swab samples, the multiplexed electrical detection assay shows an identification accuracy of 97.1% for the discrimination of SARS-CoV-2 variants. Our designed multiplexed electrical detection assay with SNP identification capability provides an efficient tool to achieve scalable pandemic screening.

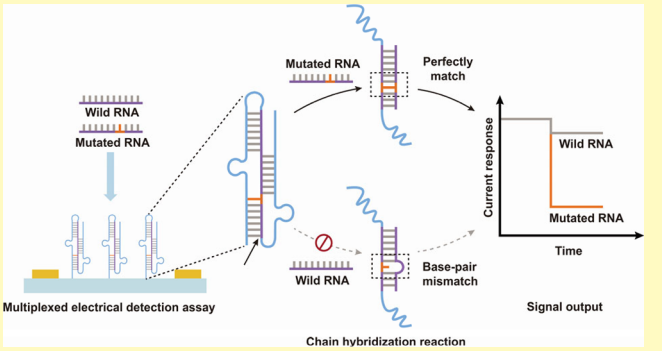

KEYWORDS: *DNA probes, biosensors, nanodevices, single-nucleotide polymorphism, RNA mutations*

The pandemic and evolution of the coronavirus disease 2019 (COVID-19) have brought about major challenges to global public health and economic development.[1] Since the first emergence of the severe acute respiratory syndrome coronavirus 2 (SARS-CoV-2) variant with D614G mutation, a typically single-nucleotide polymorphism (SNP) in the viral genome, SARS-CoV-2 has evolved in a rapid mutating manner into multiple variant strains with different transmissibility, pathogenicity, and vaccine efficacy.[2] For instance, the Alpha (B.1.1.7) variant shows an increased transmission rate of 50% compared with the original strain.[3,4] The Beta (B.1.351) variant gave rise to a reduction of trial efficacy of the AZD1222 vaccine from 70 to 10%.[5] The Delta (B.1.617.2) variant was reported to be 60% more transmissible than the Alpha variant.[6,7] Notably, Omicron (BA.1) and its sublineages (BA.4 and BA.5) show a particularly large number of mutations (>30 mutations) in its spike, significantly increasing their transmission rate and reducing the vaccine protective efficacy.[8,9] Thus, it is of great significance to differentiate SARS-CoV-2 variants, especially for variants of concern (VOCs), which are recommended by the World Health Organization (WHO), for the accurate evaluation of viral transmission rate and pathogenicity, as well as to curb viral transmission and develop an efficient vaccine.[10,11]

An ideal method for scalable screening and identification of SARS-CoV-2 variants should be possessed several critical characteristics: (i) Sensitively detecting RNA mutations in the SARS-CoV-2 genome at single-nucleotide resolution. Generally, the SARS-CoV-2 variants differed in several nucleotides or even single-nucleotide mutation, and the thermodynamic stability difference between single-nucleotide mutated sequences and sequences without mutations is particularly negligible.[12−15] (ii) Rapid readout of detection results. Currently developed methods for the identification of SARS-CoV-2 variants require a time-consuming nucleic acid amplification process, and the turnaround time from sample-to-result costs at least 30 min, making it inadaptable for rapid and scalable variants screening.[16−18] (iii) Capable of detecting multiplexed RNA mutations simultaneously. SARS-CoV-2 VOCs involve a huge number of sublineages and sets of corresponding RNA mutations.[2,9,19] The detection of multiple mutated RNAs

Received: March 8, 2023
Accepted: May 5, 2023
Published: May 17, 2023

Scheme 1. Schematic of the Structure of PNprobe and The Identification of SARS-CoV-2 Variants with PNprobe-Functionalized FET Biosensors

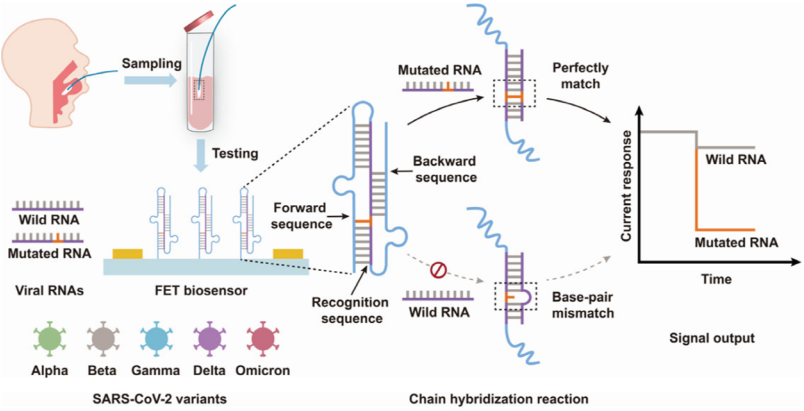

simultaneously is expected to improve the identification efficiency of RNA mutations and the ability in differentiating SARS-CoV-2 variants.[20−23] Therefore, the development of an efficient nucleic acid detection assay with the capability to accurately identify viral genome SNPs is highly demanded to achieve rapid SARS-CoV-2 variants screening.

Here, we proposed a multiplexed electrical detection assay based on a paperclip-shaped nucleic acid probe (PNprobe) functionalized field-effect transistor (FET) biosensor for specific identification of RNA mutations with single-nucleotide resolution to achieve rapid screening of SARS-CoV-2 variants. The three-stem structure designed in the PNprobe prominently increases the thermodynamic stability of probes and amplifies the thermodynamic stability difference between variant RNAs that differ in a single-nucleotide mutation. The specific recognition of viral RNA with the single-nucleotide mutation was electrically read out by FET biosensors within 15 min. Notably, the developed multiplexed electrical detection assay shows the capability in the highly sensitive detection of mutated RNA with a limit of detection (LOD) down to 0.03 copies μL^{-1}. With the assistance of 8 FET detection channels, the developed multiplexed electrical detection assay achieves the detection of 7 mutated RNAs and shows a 97.1% accuracy in the discrimination of 5 SARS-CoV-2 VOCs for 70 simulated SARS-CoV-2 positive throat swab samples. Our designed assay provides an effective tool for single-nucleotide mutation detection and a strategy for large-scale epidemic screening.

EXPERIMENTAL SECTION

Materials. Methanol, ethanol, acetone, and ammonium persulfate were purchased from Sinopharm Chemical Reagent Co., Ltd. Sulfosuccinimidyl 4-(*N*-maleimidomethyl)cyclohexane-1-carboxylate (Sulfo-SMCC), poly(methyl methacrylate) (PMMA), (3-Aminopropyl)triethoxysilane (APTES), acrylamide, bis-acrylamide, *N*,*N*,*N*′,*N*′-Tetramethylethylenediamine (TEMED), and tris-borate-edetate disodium (TBE) buffer were obtained from Aladdin. BSA, 1 × PBS (1 × 10^{-2} M, pH 7.4), and nuclease-free water were provided by Shanghai Yuanye Bio-Technology Co., Ltd. 10 × GelRed and viral transport medium (VTM) were purchased from Wuhan Servicebio Technology Co., Ltd. DNA and RNA oligonucleotides were obtained from Sangon and purified by high-performance liquid chromatography (HPLC). The full-genome RNA standards were purchased from the National Institute of Metrology (China), which were obtained through in vitro transcription, containing the complete genomic fragments of SARS-CoV-2 N gene, E gene, S gene, and ORF1ab gene.

Instruments and Characterizations. The isothermal titration calorimetry (ITC) experiments were performed on an isothermal titration calorimeter (MicroCal PEAQ-ITC, Britain). The images of gel electrophoresis were scanned by a gel imaging system (ChemiDoc XRS+, America). The electrodes (Cr/Au, 10 nm/30 nm) array of FET was patterned by ultraviolet (UV) lithography (ABM. Inc., America). The indium gallium zinc oxide (IGZO) channel materials were deposited by a thermal evaporator system (Jiashuo JSD300-II, China) with the assistance of metallic mask templates. The sensing region of the FET biosensor was exposed by an electron beam lithography system (EBL, JSM-6510, Japan) after PMMA protection. The modification of PNprobe on the IGZO surface was characterized by attenuated total reflection Fourier transformed infrared spectroscopy (ATR-FTIR, FTIR5700, USA). The surface morphologies of FET biosensors were characterized by atomic force microscopy (AFM, Park nx10, Korea). The photograph of the multiplexed electrical detection nanodevice was obtained using a camera (Nikon D7100, Japan). The electrical characteristics of the IGZO FET biosensors and multiplexed electrical detection devices were measured by a digital source meter (Keysight B1500A, Germany) connected to a probe station (PRCBE LAB, China). More details on the IGZO FET devices fabrication and testing could be found in the Supporting information.

Analysis of the Binding Affinity of PNprobe with ITC. The binding affinity of PNprobe was evaluated with ITC operated on MicroCal PEAQ-ITC at 25 °C. PNprobes and all the measured RNAs were dissolved in 1 × PBS. The testing was performed by adding 2 μL measured RNAs (2 μM) continuously into the cell containing 10 μM PNprobe for 19 times with a 2.5 min interval time. The titration data were analyzed by using ITC data processing software (MicroCal PEAQ-ITC Analysis Software).

Polyacrylamide Gel Electrophoresis (PAGE). Samples with PNprobe (2 μM) only, mutated RNA (5 μM) only, wild RNA (5 μM) only, and PNprobe (2 μM) hybridized with mutated RNA (5 μM) or wild RNA (10 μM) (total reaction-mixture volume: 10 μL) were equilibrated for 30 min at 25 °C and then analyzed on a 20% polyacrylamide gel at 130 V in 1 × TBE buffer for 90 min. The gel was stained in 3 × GelRed nucleic acid stain solution for 20 min and imaged with ChemiDoc XRS+.

Preparation of Simulated Throat Swab Samples. The synthetic RNAs of three coronaviruses, including SARS-CoV-2, severe acute respiratory syndrome coronavirus (SARS-CoV), and middle east respiratory syndrome coronavirus (MERS-CoV), were centrifuged at 3000 rpm at 4 °C for 5 min and then diluted into a concentration of 5000 copies μL^{-1} with VTM containing 2% RNase inhibitor. Subsequently, these viral RNAs were then further diluted with negative throat swab samples to obtain simulated SARS-CoV-2, SARS-CoV, and MERS-CoV positive throat swab samples with a concentration of 100 copies μL^{-1}. The full-genome RNA standards of SARS-CoV-2 wild strain and variants were centrifuged at 3000 rpm at

https://doi.org/10.1021/acssensors.3c00453
ACS Sens. 2023, 8, 2096−2104

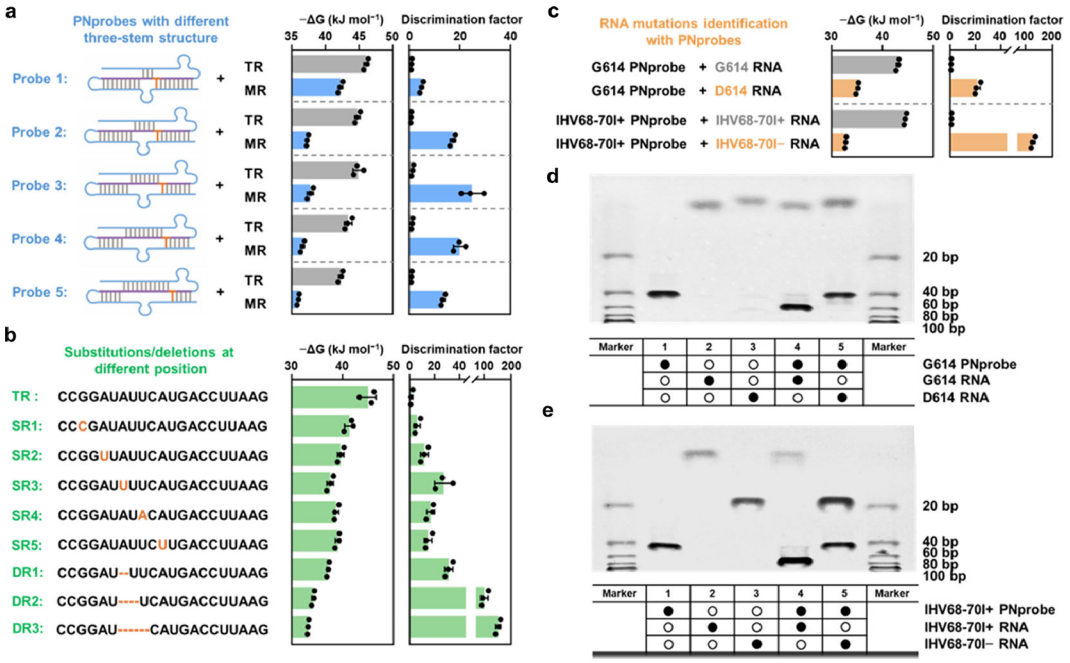

Figure 1. Design and optimization of PNprobes for the identification of RNA mutations at single-nucleotide resolution. (a) Identification of SNPs using PNprobes with different three-stem structures. Shown are the diagrams of the PNprobe structure. TR, target RNA; MR, mismatched RNA. (b) Identification of nucleotide substitutions and deletions using PNprobes with a 7-7-7 bps three-stem structure. SR, substituted RNA; DR, deleted RNA. (c) Identification of D614G and IHV68-70I RNA mutations using G614 PNprobe and IHV68-70I + PNprobe. $-\Delta G$ and discrimination factors in data a, b, and c were calculated through the ITC measurement. (d) Electrophoretic analysis of the G614 PNprobe binding G614 and D614 RNA sequences. (e) Electrophoretic analysis of the IHV68-70I+ PNprobe binding IHV68-70I+ and IHV68-70I− RNA sequences. Data in a, b, and c were expressed as mean ± s.d. (n = 3).

4 °C for 5 min and then diluted into negative throat swab samples to obtain simulate SARS-CoV-2 positive throat swab samples with unknown RNA concentrations.

RESULTS AND DISCUSSION

Design and Working Principle of PNprobe-Functionalized FET Biosensors. Scheme 1 presents the structure of designed PNprobes and the working principle of probes functionalized FET devices for SARS-CoV-2 variants' mutated RNA detection. The PNprobe comprises three parts, including forward sequence, recognition sequence, and backward sequence. The recognition sequence is fully complementary to mutated RNA with 21 nucleotides in length for specific recognition and binding. The forward and backward sequences are devised to be complementary and paired to different parts of the recognition sequence to form a stabilized three-stem structure in PNprobes. The three-stem structure equips the PNprobe with exceptional thermodynamic stability, which could only be disrupted when exposed to mutated RNA. Whereas, in the presence of wild RNA, the three-stem structure of PNprobes could not be destabilized owing to the thermodynamic energy penalty derived by single-base mismatch, leading to a failure of the biorecognition event. By incorporating PNprobes onto the interface of FET biosensors, the specific recognition event of PNprobe with mutated RNA is rapidly amplified and converted into a readable electrical signal. With the integration of PNprobe-functionalized FET units, a multiplexed electrical detection assay is constructed to detect 7 mutated RNAs for the achievement of SARS-CoV-2 VOCs discrimination.

Design and Performance Evaluation of PNprobe. To obtain an optimized PNprobe, the three-stem length and the position of base-pairing mismatch in the recognition sequence on the binding affinity of PNprobes were investigated. The designed five PNprobes contain a three-stem structure of 9-3-9 base-pairs (bps) (PNprobe1), 8-5-8 bps (PNprobe2), 7-7-7 bps (PNprobe3), 6-9-6 bps (PNprobe4), and 5-11-5 bps (PNprobe5), respectively (Figure 1a and Table S1). The ratio of binding constants (K_a) of PNprobes to target RNA (TR) and single-base mismatched RNA (MR) was defined as the discrimination factor to assess the binding affinity of PNprobe. According to the ITC measurement results, the discrimination factors and Gibbs free energy changes (ΔG) of five PNprobes after binding with TR and MR were calculated (Figure S1).[24−26] Among the designed PNprobes, PNprobe3 shows a much lower ΔG (−45.7 kJ/mol) and the highest discrimination factor (up to 26.2) upon binding to TR, indicating that PNprobe3 with a 7-7-7 bps three-stem structure exhibits a strong binding ability to TR (Figure 1a). Moreover, the generated ΔG of all designed PNprobes are significantly higher toward MR compared to TR, suggesting the amplified thermodynamic stability difference of PNprobes to TR and MR owing to the three-stem structure. Subsequently, the position of base-pairing mismatch in the recognition sequence was optimized by introducing single-base substitutions at the 3, 5, 7, 9, and 11 nt (donated as SR1 to SR5, Figure 1b). Notably, when the single-base mismatch position was set at 7 nt, the PNprobe with 7-7-7 bps three-stem structure shows a remarkably large ΔG (−37.6 kJ/mol) upon binding to single-base mismatch RNA compared to TR. Similarly, the PNprobe can effectively distinguish TR from single-base, double-base, and triple-base deletion RNA sequences (donated as DR1, DR2, and DR3, respectively). The above results demonstrate that PNprobes with 7-7-7 bps three-stem

https://doi.org/10.1021/acssensors.3c00453
ACS Sens. 2023, 8, 2096−2104

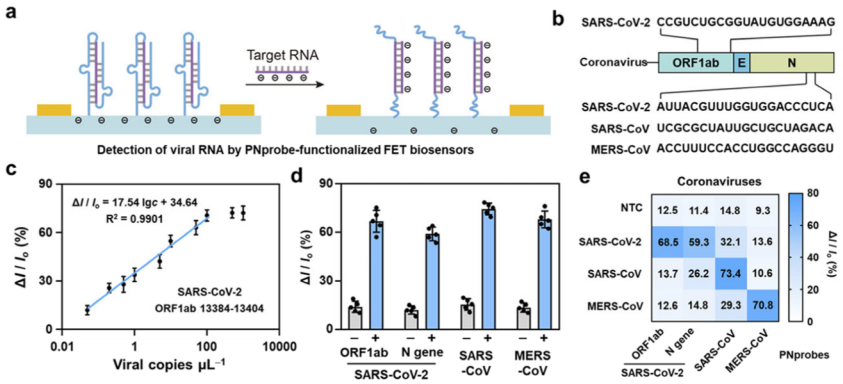

Figure 2. Identification of viral RNA with PNprobe-functionalized FET biosensors. (a) Schematic illustration of the working principle of PNprobe-functionalized FET biosensors. (b) Parts genome map of three coronaviruses and the selected targeted gene regions. (c) Current responses of PNprobe-functionalized FET biosensors to SARS-CoV-2 ORF1ab gene with concentrations ranging from 0.05 to 1000 copies μL^{-1}. (d) Current responses of PNprobe-functionalized FET biosensors to simulated throat swab samples spiked with 100 copies μL^{-1} RNAs of three coronaviruses. The simulated SARS-CoV-2 positive throat swab samples contain 100 copies μL^{-1} SARS-CoV-2 ORF1ab gene and N gene. Data in (c) and (d) were expressed as mean ± s.d. (n = 3). (e) Cross-reaction test of simulated SARS-CoV-2, SARS-CoV, and MERS-CoV positive samples by four PNprobes functionalized FET biosensors, respectively. NTC, no target control.

structure and single-base mismatch located at 7 nt in the recognition sequence exhibit the optimized discrimination capability for RNA that differs in a single-nucleotide mutation.

To estimate the capability and applicability of the optimized PNprobe in detecting RNA mutations of SARS-CoV-2 variants, two representative RNA mutations in the SARS-CoV-2 genome, including D614G and IHV68-70I mutations were selected for the following measurements.[27,28] We designed two PNprobes (G614 PNprobe and IHV68-70I + PNprobe) that are specific to D614G and IHV68-70I mutated RNA and evaluate their discrimination factors to mutated and wild RNA. As indicated in Figure 1c, the calculated discrimination factors of the two PNprobes were up to 21.5 and 181.6, respectively, reflecting the remarkable capability of the designed PNprobes in distinguishing mutated RNA from wild RNA. Additionally, an obvious gel band was observed in the image of gel electrophoresis when the PNprobe was exposed to mutated RNA (Figure 1d,e). By contrast, there is no new gel band observed in the lane of PNprobe and wild RNA even when the concentration of wild RNA is 5 times that of mutated RNA. The above results indicate that the designed PNprobe with optimized structure is capable of specifically recognizing mutated viral RNA at single-nucleotide resolution.

Identification of Viral RNA with PNprobe-Functionalized FET Biosensors. To examine the detection performance of the PNprobe toward SARS-CoV-2 RNA, sulfydryl-functionalized PNprobes (SH-PNprobes) were introduced onto the amination-treated sensing interface of IGZO FET by Sulfo-SMCC cross-linking reagent (Figures 2a and S2). In the presence of target viral RNA with negative charges, the PNprobe immobilized on the IGZO sensing interface could recognize and combine with target viral RNA, resulting in a change of charge density on the FET biosensing interface. The biorecognition event between the PNprobe and target viral RNA is subsequently amplified by the IGZO FET device and converted into a readable electrical signal. The presence of absorption peaks corresponding to amido bonds (1560 and 1650 cm^{-1}) and phosphate skeleton of the nucleic acid probe (1240 cm^{-1}) in the ATR-FTIR curves verify that the PNprobe was successfully immobilized on the FET biosensing interface (Figure S3).[22,29] The AFM characterization indicates a uniform and vertical PNprobe functional layer formed on the FET channel surface with an average height of about 9.1 nm, which is consistent with the theoretical vertical height of PNprobe (Figure S4).[30−32] Additionally, the transfer characteristic curve of the FET biosensor at a fixed source-drain voltage (V_d) under the liquid-gate bias (V_g) shows an obvious right shift after the PNprobe functionalization (Figure S5a), which can be attributed to the charge repulsion effect of the negatively charged PNprobes on carriers in the FET channel.[33−35] The real-time current response curve reveals that the PNprobe-functionalized FET biosensor maintains a relatively stable current over long-term monitoring (Figure S5b). The above results demonstrate that the PNprobe was successfully immobilized on the FET interface and shows excellent stability.

Next, three coronaviruses, including SARS-CoV-2, SARS-CoV, and MERS-CoV, were selected to evaluate the detection capability of the PNprobe-functionalized FET biosensor (Figure 2b).[36,37] A series of PNprobes was designed to specifically target the corresponding gene regions (Table S2). An optimized PNprobe modification concentration (1 μM) and viral RNA incubation time of 5 min were selected for the subsequent measurements (Figure S6). The current response ($100 \times \Delta I_d/I_o$) that was defined as the ratio of the current change (ΔI_d) before and after target viral RNA conjugation to the initial current (I_o) was adopted to evaluate the detection capability of the PNprobe-functionalized IGZO FET biosensor. As illustrated in Figure 2c, with the concentration of SARS-CoV-2 ORF1ab RNA increasing from 0.05 to 100 copies μL^{-1}, the current responses exhibit a linear increase. Other PNprobe-functionalized FET biosensors that are specific to N gene regions of SARS-CoV-2, SARS-CoV, and MERS-CoV show a similar detection performance to the corresponding target viral RNA (Figures S8 and S9). According to the current response curves, the calculated LOD was calculated as the concentration generating a $|\Delta I_d/I_o|$ response equal to three times the average noise level. Thus, the LOD of the PNprobe-functionalized FET biosensors to the SARS-CoV-2 ORF1ab gene, SARS-CoV-2 N gene, SARS-CoV N gene, and MERS-CoV N gene are 0.03, 0.14, 0.05, and 0.10 copies μL^{-1}, respectively. The extremely low detection limit indicates that the designed PNprobe-functionalized FET biosensor is

https://doi.org/10.1021/acssensors.3c00453
ACS Sens. 2023, 8, 2096−2104

accessible to be applied for highly sensitive detection of coronavirus RNAs.

In order to evaluate the applicability of the PNprobe-functionalized FET biosensor in practical sample detection, several simulated throat swab samples spiked with viral RNAs of three coronaviruses, were detected. As shown in Figure 2d, the observed current responses of all PNprobe-functionalized FET biosensors to target viral RNAs are more than 55%, suggesting the excellent sensitivity of our developed FET biosensors in detecting coronavirus RNAs in practical samples. Notably, the whole detection time only requires ~15 min due to the rapid response of the FET biosensor, suggesting that the PNprobe-functionalized FET biosensor shows potential in point-of-care detection (Figure S10). Given that the viral genomes of three coronaviruses share a high degree of similarity,[37] a cross-reaction test was performed to challenge the specificity of the PNprobe-functionalized IGZO FET biosensor. As shown in Figure 2e, the FET biosensor with SARS-CoV-2 ORF1ab gene-specific PNprobe shows a remarkable current response of 65.8% to SARS-CoV-2 positive throat swab samples. In contrast, the current responses of the biosensors to SARS-CoV and MERS-CoV positive throat swab samples were 8.7 and 10.6%, respectively. Similar detection results were observed in other FET biosensors that were specific to the N gene of three tested coronaviruses (Figure 2e). The above results reveal that the developed PNprobe-functionalized FET biosensor features excellent detection sensitivity and specificity in practical samples and could be utilized in the rapid detection and effective discrimination of SARS-CoV-2, SARS-CoV, and MERS-CoV.

Identification of RNA Mutations in SARS-CoV-2. To investigate the detection ability of PNprobe-functionalized FET biosensors for different RNA mutations in SARS-CoV-2 variants, seven representative RNA mutations, including SNPs, such as K417N, K417T, and D614G mutations, as well as mutations with nucleotide deletion, such as LPPA24-27S, IHV68-70I, GVYY142-145D, and EFR156-158G were considered (Figures 3a and S12).[2,38−40] Figures 3b,c and S11 display the current responses of the PNprobe-functionalized FET biosensors toward D614G mutation and IHV68-70I mutation, respectively. Obviously, the current responses increase gradually with the concentration of mutated RNA. For 1 copies μL^{-1} mutated RNA, the two FET biosensors produce significant current responses of 31.6 and 34.3%, respectively, while only 20.6 and 13.2% current responses were generated for 1000 copies μL^{-1} wild RNA. It reflects that PNprobe-functionalized FET biosensors could achieve highly sensitive identification of mutated RNA even at an extremely low concentration.

For the mutated and wild RNA with the same concentration, seven PNprobe-functionalized FET biosensors specific to different RNA mutations show a 3-6-fold higher current response to mutated RNA than wild RNA (Figures 3d and S13). The excellent current response suggests that the developed FET biosensor is capable of identifying multiple mutated gene sequences in SARS-CoV-2 variants with high sensitivity.

For investigating the capability of PNprobe-functionalized FET biosensors in detecting RNA mutations in the full genomes of SARS-CoV-2 variants, four PNprobe-functionalized FET biosensors that were specific to D614, G614, IHV68-70I−, and IHV68-70I+ wild or mutated RNA were designed to detect the RNA standards of wild-type, Alpha, and

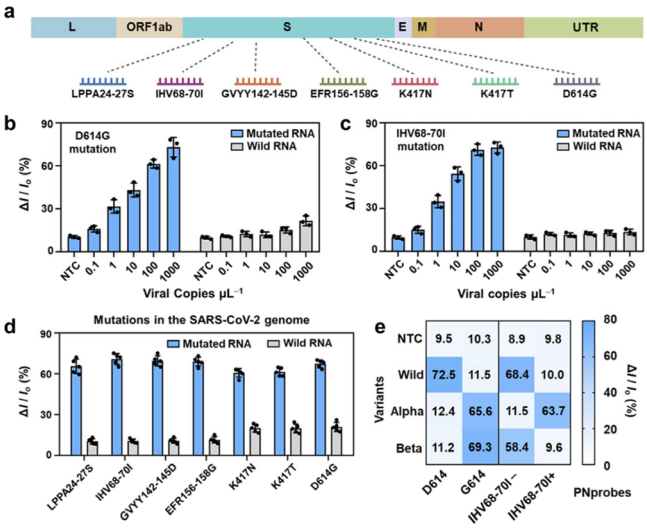

Figure 3. Detection of SARS-CoV-2 RNA mutations, including nucleotide substitutions and deletions. (a) SARS-CoV-2 genome map and the selected RNA mutations. Current responses of PNprobe-functionalized FET biosensors to (b) SARS-CoV-2 D614G mutation and (c) IHV68-70I mutation with concentrations of mutated and wild RNAs ranging from 0.1 to 1000 copies μL^{-1}. (d) Current responses of PNprobe-functionalized FET biosensors toward seven mutations in the mutated and wild RNA. The concentration of viral RNA is 100 copies μL^{-1}. (e) Current responses of FET biosensors functionalized with D614G and IHV68-70I mutations specific PNprobes toward wild and two representative mutated RNA standards. The concentrations of full-genome RNA standards are 100 copies μL^{-1}. NTC, no target control. Data in (b) and (c) were expressed as mean ± s.d. (n = 3). Data in (d) were expressed as mean ± s.d. (n = 5).

Beta variants (Table S1). Figure 3e shows that D614G and IHV68-70I mutated RNAs were not detected in the wild-type RNA standards, while they were observed in the Alpha variant. For the Beta variant, the D614G mutated RNA and wild RNA of IHV68-70I mutation were detected. These measurement results are consistent with RNA mutations in Alpha and Beta variants certified by the CDC and reported in the literature,[19] demonstrating that the PNprobe-functionalized FET biosensor could effectively identify RNA mutations in the full-genome of SARS-CoV-2 variants.

Identification of SARS-CoV-2 Variants with Multiplexed Electrical Detection Assay. A multiplexed electrical detection nanodevice consisting of eight PNprobe-functionalized FET biosensors was designed to identify various SARS-CoV-2 variants simultaneously (Figure 4a). In the multiplexed electrical detection nanodevice, channel 2 to channel 8 were designed to target D614G, IHV68-70I, K417N, K417T, EFR156-158G, GVYY142-145D, and LPPA24-27S mutations, respectively. Channel 1 was modified with PNprobes targeting the human RNase P gene present in human throat swab samples. The presence of the RNase P gene reflects the successful sampling of throat swab samples and the reliability of detection results.[15]

The relationships between seven RNA mutations and SARS-CoV-2 variants are illustrated in Figure 4b. The synthetic full-genome RNA standards of wild-type SARS-CoV-2 and five variants (Alpha, Beta, Gamma, Delta, and Omicron BA.1) were spiked into negative throat swab samples for the variant identification evaluation. Figure 4c shows the current responses of multiplexed electrical detection nanodevices toward seven mutations in RNA standards corresponding to

https://doi.org/10.1021/acssensors.3c00453
ACS Sens. 2023, 8, 2096−2104

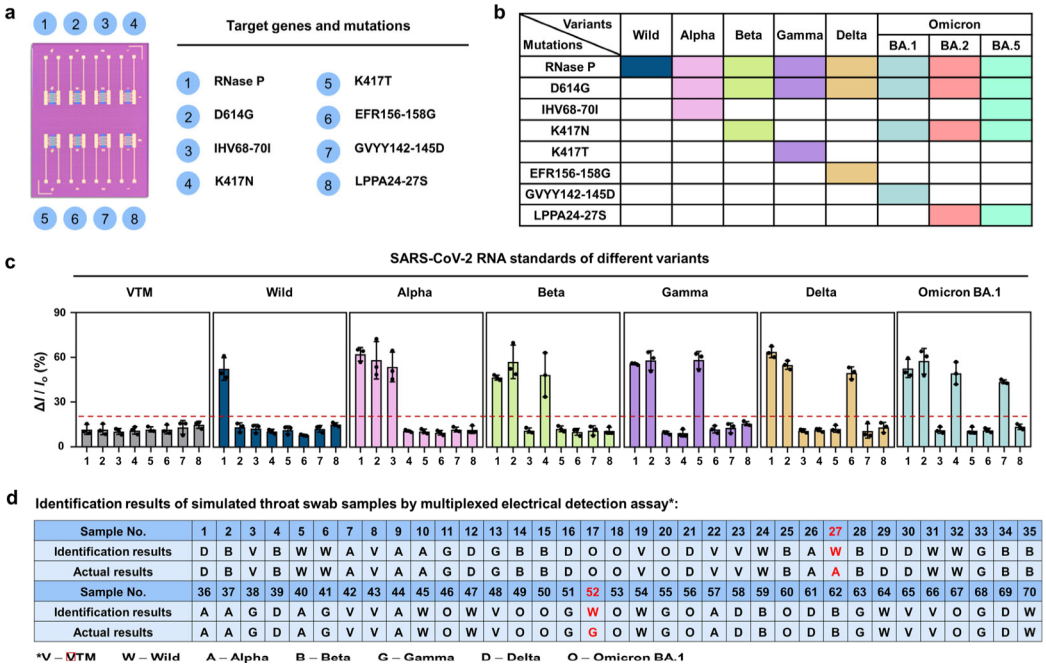

Figure 4. Discrimination of SARS-CoV-2 variants with multiplexed electrical detection assay. (a) Digital photograph and the FET detection channels of the multiplexed electrical detection nanodevice. (b) The relationship between the mutations and different SARS-CoV-2 variants. (c) Current responses of the multiplexed electrical detection assay to simulated positive throat swab samples spiked with 100 copies μL^{-1} full-genome RNA standards of five SARS-CoV-2 variants and wild-type SARS-CoV-2. VTM, viral transport medium. (d) Identification results of SARS-CoV-2 and its variants for 70 simulated positive throat swab samples with multiplexed electrical detection assay. The incorrect discrimination results are labeled in red. Data in (c) were expressed as mean ± s.d. (n = 3).

different variants. It can be observed that the current responses of multiplexed detection nanodevices are significantly different for the presence and absence of target RNA mutations. According to Figure 3b, a 20% cut-off value was determined to indicate a significant difference generated between the mutated RNA and wild RNA whose content is even 1000 times higher. Specifically, for the Beta variant, the current responses of channels 1, 2, and 4 that were corresponding to RNase P gene, D614G, and K417N mutations are significantly higher than the cut-off value (20%), suggesting that the multiplexed electrical detection nanodevice is capable of correctly identifying D614G and K417N mutations present in Beta variant. The multiplexed electrical detection nanodevice also correctly identifies SARS-CoV-2 variants, including Gamma, Delta, and Omicron BA.1. These results indicate that the multiplexed electrical detection assay can simultaneously detect multiple mutations in the full-genome viral RNA of SARS-CoV-2 variants to realize effective variants discrimination.

Subsequently, to estimate the detection capability of multiplexed electrical detection assay in practical applications, 60 simulated SARS-CoV-2 positive throat swab samples with wild-type virus and five variants mentioned above were prepared by adding the corresponding RNA standards into negative throat swab samples and tested with the multiplexed electrical detection assay. Ten samples without any target were used as blank controls. Figures 4d and S14 show the measurement results of multiplexed electrical detection assay on 70 simulated throat swab samples. For each simulated sample, the existence of relevant RNA mutations was determined according to the current responses of the corresponding mutated RNA detection channel. The variants were then determined by the relationship between the RNA mutations and viral lineages depicted in Figure 4b. A statistical result shows that the multiplexed electrical detection assay correctly discriminates 68 samples out of 70 simulated samples, with an accuracy of 97.1% (Figure S15). Additionally, the obtained current responses showed a semi-quantitative correlation with the reverse transcription-quantitative polymerase chain reaction (RT-qPCR) test results, reflecting the comparable diagnostic performance of our multiplexed electrical assay compared with the gold standard (Figures S16 and S17). Notably, it cost less than 15 min for the multiplexed electrical detection assay to test each simulated throat swab sample, including sampling, incubation, testing, and output results (Figure S18). The above results indicate that the multiplexed electrical detection assay shows great potential as a point-of-care test for large-scale screening and identification of SARS-CoV-2 variants.

CONCLUSIONS

In conclusion, a multiplexed electrical detection assay based on FET biosensors functionalized with a three-stem structured PNprobe was designed to detect RNA mutations of the SARS-CoV-2 genome at single-nucleotide resolution, to achieve SARS-CoV-2 variants discrimination. The three-stem structure significantly amplified the thermodynamic stability difference between variant RNAs that differ in single-nucleotide mutations, thus improving the binding ability of the PNprobe to target RNA compared to single-base mismatch RNA. The developed multiplexed electrical detection nanodevice shows a short turnaround time from sample to result (<15 min) and high sensitivity (LOD of 0.03 copies μL^{-1}) in detecting mutated RNA of SARS-CoV-2 variants. With the assistance of eight combinatorial FET detection channels, the multiplexed electrical detection assay shows the capability to identify key RNA mutations and achieve various SARS-CoV-2 variants

https://doi.org/10.1021/acssensors.3c00453
ACS Sens. 2023, 8, 2096−2104

discrimination simultaneously. For 70 simulated throat swab samples, the developed multiplexed electrical detection assay shows a 97.1% discrimination accuracy in identifying SARS-CoV-2 variants. Considering the programmability of the PNprobe, an effective multiplexed RNA detection assay could be developed through rationally designed PNprobes, which is expected to be applied for large-scale and rapid screening of infectious diseases caused by multiple RNA viruses.

■ ASSOCIATED CONTENT

Supporting Information

The Supporting Information is available free of charge at https://pubs.acs.org/doi/10.1021/acssensors.3c00453.

Details of IGZO FET nanodevice design, fabrication and testing, thermodynamic analysis, characterization, transfer characteristic curves and current responses of nanodevices to samples, performance comparison, and lists of DNA and RNA oligonucleotides used in this work (PDF)

■ AUTHOR INFORMATION

Corresponding Authors

Yanbing Yang − *College of Chemistry and Molecular Sciences, Key Laboratory of Biomedical Polymers of Ministry of Education, Institute of Molecular Medicine, Renmin Hospital of Wuhan University, School of Microelectronics, Wuhan University, Wuhan 430072, P. R. China*; Email: yangyanbing@whu.edu.cn

Quan Yuan − *College of Chemistry and Molecular Sciences, Key Laboratory of Biomedical Polymers of Ministry of Education, Institute of Molecular Medicine, Renmin Hospital of Wuhan University, School of Microelectronics, Wuhan University, Wuhan 430072, P. R. China; Molecular Science and Biomedicine Laboratory (MBL), State Key Laboratory of Chemo/Biosensing and Chemometrics, College of Chemistry and Chemical Engineering, Hunan University, Changsha 410082, P. R. China;* orcid.org/0000-0002-3085-431X; Email: yuanquan@whu.edu.cn

Authors

Yun Zhang − *College of Chemistry and Molecular Sciences, Key Laboratory of Biomedical Polymers of Ministry of Education, Institute of Molecular Medicine, Renmin Hospital of Wuhan University, School of Microelectronics, Wuhan University, Wuhan 430072, P. R. China*

Bo Chen − *College of Chemistry and Molecular Sciences, Key Laboratory of Biomedical Polymers of Ministry of Education, Institute of Molecular Medicine, Renmin Hospital of Wuhan University, School of Microelectronics, Wuhan University, Wuhan 430072, P. R. China*

Duo Chen − *College of Chemistry and Molecular Sciences, Key Laboratory of Biomedical Polymers of Ministry of Education, Institute of Molecular Medicine, Renmin Hospital of Wuhan University, School of Microelectronics, Wuhan University, Wuhan 430072, P. R. China*

Yiming Wang − *College of Chemistry and Molecular Sciences, Key Laboratory of Biomedical Polymers of Ministry of Education, Institute of Molecular Medicine, Renmin Hospital of Wuhan University, School of Microelectronics, Wuhan University, Wuhan 430072, P. R. China*

Qingqing Lu − *College of Chemistry and Molecular Sciences, Key Laboratory of Biomedical Polymers of Ministry of Education, Institute of Molecular Medicine, Renmin Hospital of Wuhan University, School of Microelectronics, Wuhan University, Wuhan 430072, P. R. China*

Jie Tan − *Molecular Science and Biomedicine Laboratory (MBL), State Key Laboratory of Chemo/Biosensing and Chemometrics, College of Chemistry and Chemical Engineering, Hunan University, Changsha 410082, P. R. China;* orcid.org/0000-0002-0909-2904

Long Chen − *Department of Computer and Information Science, Faculty of Science and Technology, University of Macau, Macau 999078, P. R. China*

Liping Zhou − *College of Chemistry and Molecular Sciences, Key Laboratory of Biomedical Polymers of Ministry of Education, Institute of Molecular Medicine, Renmin Hospital of Wuhan University, School of Microelectronics, Wuhan University, Wuhan 430072, P. R. China*

Weihong Tan − *Molecular Science and Biomedicine Laboratory (MBL), State Key Laboratory of Chemo/Biosensing and Chemometrics, College of Chemistry and Chemical Engineering, Hunan University, Changsha 410082, P. R. China*

Complete contact information is available at: https://pubs.acs.org/10.1021/acssensors.3c00453

Author Contributions

Y.Z., B.C., and D.C. contributed equally to this work. All authors have given approval for the final version of the manuscript.

Funding

The authors kindly acknowledge the support from the National Natural Science Foundation of China (21925401), the National Key R&D Program of China (2021YFA1202400), the Fundamental Research Funds for the Central Universities (2042022rc0004), and the Tencent Foundation.

Notes

The authors declare no competing financial interest.

■ ACKNOWLEDGMENTS

We thank the Core Facility of Wuhan University for ATR-FTIR and ITC analysis. The study was approved by the Ethics Committee of Renmin Hospital of Wuhan University (WDRY2022-K257).

■ REFERENCES

(1) Phelan, A. L. COVID-19 Immunity Passports and Vaccination Certificates: Scientific, Equitable, and Legal Challenges. *Lancet* **2020**, *395*, 1595−1598.

(2) Harvey, W. T.; Carabelli, A. M.; Jackson, B.; Gupta, R. K.; Thomson, E. C.; Harrison, E. M.; Ludden, C.; Reeve, R.; Rambaut, A.; Peacock, S. J.; et al. SARS-CoV-2 Variants, Spike Mutations and Immune Escape. *Nat. Rev. Microbiol.* **2021**, *19*, 409−424.

(3) Liu, Y.; Liu, J.; Plante, K. S.; Plante, J. A.; Xie, X.; Zhang, X.; Ku, Z.; An, Z.; Scharton, D.; Schindewolf, C.; et al. The N501Y Spike Substitution Enhances SARS-CoV-2 Infection and Transmission. *Nature* **2022**, *602*, 294−299.

(4) Port, J. R.; Yinda, C. K.; Avanzato, V. A.; Schulz, J. E.; Holbrook, M. G.; van Doremalen, N.; Shaia, C.; Fischer, R. J.; Munster, V. J. Increased Small Particle Aerosol Transmission of B.1.1.7 Compared with SARS-CoV-2 Lineage A in Vivo. *Nat. Microbiol.* **2022**, *7*, 213−223.

(5) Madhi, S. A.; Baillie, V.; Cutland, C. L.; Voysey, M.; Koen, A. L.; Fairlie, L.; Padayachee, S. D.; Dheda, K.; Barnabas, S. L.; Bhorat, Q. E.; et al. Efficacy of the ChAdOx1 nCoV-19 Covid-19 Vaccine Against the B.1.351 Variant. *N. Engl. J. Med.* **2021**, *384*, 1885−1898.
(6) Mlcochova, P.; Kemp, S.; Dhar, M. S.; Papa, G.; Meng, B.; Mishra, S.; Whittaker, C.; Mellan, T.; Ferreira, I.; Datir, R.; et al. SARS-CoV-2 B.1.617.2 Delta Variant Emergence, Replication and Sensitivity to Neutralising Antibodies. *bioRxiv* **2021**, DOI: 10.1101/2021.05.08.443253.
(7) Planas, D.; Veyer, D.; Baidaliuk, A.; Staropoli, I.; Guivel-Benhassine, F.; Rajah, M. M.; Planchais, C.; Porrot, F.; Robillard, N.; Puech, J.; et al. Reduced Sensitivity of SARS-CoV-2 Variant Delta to Antibody Neutralization. *Nature* **2021**, *596*, 276−280.
(8) Tegally, H.; Moir, M.; Everatt, J.; Giovanetti, M.; Scheepers, C.; Wilkinson, E.; Subramoney, K.; Makatini, Z.; Moyo, S.; Amoako, D. G.; et al. Emergence of SARS-CoV-2 Omicron Lineages BA.4 and BA.5 in South Africa. *Nat. Med.* **2022**, *28*, 1785−1790.
(9) Huang, X.; Kon, E.; Han, X.; Zhang, X.; Kong, N.; Mitchell, M. J.; Peer, D.; Tao, W. Nanotechnology-Based Strategies Against SARS-CoV-2 Variants. *Nat. Nanotechnol.* **2022**, *17*, 1027−1037.
(10) Yang, J.; Song, Y.; Deng, X.; Vanegas, J. A.; You, Z.; Zhang, Y.; Weng, Z.; Avery, L.; Dieckhaus, K. D.; Peddi, A.; et al. Engineered LwaCas13a with Enhanced Collateral Activity for Nucleic Acid Detection. *Nat. Chem. Biol.* **2023**, *19*, 45−54.
(11) Casati, B.; Verdi, J. P.; Hempelmann, A.; Kittel, M.; Klaebisch, A. G.; Meister, B.; Welker, S.; Asthana, S.; Di Giorgio, S.; Boskovic, P.; et al. Rapid, Adaptable and Sensitive Cas13-Based COVID-19 Diagnostics Using ADESSO. *Nat. Commun.* **2022**, *13*, 3308.
(12) Zhao, Y.; Chen, F.; Li, Q.; Wang, L.; Fan, C. Isothermal Amplification of Nucleic Acids. *Chem. Rev.* **2015**, *115*, 12491−12545.
(13) Chen, F.; Zhao, Y.; Fan, C.; Zhao, Y. Mismatch Extension of DNA Polymerases and High-Accuracy Single Nucleotide Polymorphism Diagnostics by Gold Nanoparticle-Improved Isothermal Amplification. *Anal. Chem.* **2015**, *87*, 8718−8723.
(14) Li, Q.; Wu, J.; Nie, J.; Zhang, L.; Hao, H.; Liu, S.; Zhao, C.; Zhang, Q.; Liu, H.; Nie, L.; et al. The Impact of Mutations in SARS-CoV-2 Spike on Viral Infectivity and Antigenicity. *Cell* **2020**, *182*, 1284−1294.e9.
(15) Zhang, T.; Deng, R.; Wang, Y.; Wu, C.; Zhang, K.; Wang, C.; Gong, N.; Ledesma-Amaro, R.; Teng, X.; Yang, C.; et al. A Paper-Based Assay for the Colorimetric Detection of SARS-CoV-2 Variants at Single-Nucleotide Resolution. *Nat. Biomed. Eng.* **2022**, *6*, 957−967.
(16) Lu, S.; Tong, X.; Han, Y.; Zhang, K.; Zhang, Y.; Chen, Q.; Duan, J.; Lei, X.; Huang, M.; Qiu, Y.; et al. Fast and Sensitive Detection of SARS-CoV-2 RNA Using Suboptimal Protospacer Adjacent Motifs for Cas12a. *Nat. Biomed. Eng.* **2022**, *6*, 286−297.
(17) Johnston, M.; Ceren Ates, H.; Glatz, R. T.; Mohsenin, H.; Schmachtenberg, R.; Göppert, N.; Huzly, D.; Urban, G. A.; Weber, W.; Dincer, C. Multiplexed Biosensor for Point-of-Care COVID-19 Monitoring: CRISPR-Powered Unamplified RNA Diagnostics and Protein-Based Therapeutic Drug Management. *Mater. Today* **2022**, *61*, 129−138.
(18) Li, H.; Yang, J.; Wu, G.; Weng, Z.; Song, Y.; Zhang, Y.; Vanegas, J. A.; Avery, L.; Gao, Z.; Sun, H.; Chen, Y.; Dieckhaus, K. D.; Gao, X.; Zhang, Y. Amplification-Free Detection of SARS-CoV-2 and Respiratory Syncytial Virus Using CRISPR Cas13a and Graphene Field-Effect Transistors. *Angew. Chem., Int. Ed.* **2022**, *61*, No. e202203826.
(19) Tao, K.; Tzou, P. L.; Nouhin, J.; Gupta, R. K.; de Oliveira, T.; Kosakovsky Pond, S. L.; Fera, D.; Shafer, R. W. The Biological and Clinical Significance of Emerging SARS-CoV-2 Variants. *Nat. Rev. Genet.* **2021**, *22*, 757−773.
(20) Zhao, J.; Di, Z.; Li, L. Spatiotemporally Selective Molecular Imaging via Upconversion Luminescence-Controlled, DNA-Based Biosensor Technology. *Angew. Chem., Int. Ed.* **2022**, *61*, No. e202204277.
(21) Zhao, L.-D.; Yang, X.; Zhong, X.; Zhuo, Y. Advances in Electrochemiluminescence Biosensors Based on DNA Walkers. *ChemPlusChem* **2022**, *87*, No. 202200070.
(22) Yang, Y.; Wang, J.; Huang, W.; Wan, G.; Xia, M.; Chen, D.; Zhang, Y.; Wang, Y.; Guo, F.; Tan, J.; et al. Integrated Urinalysis Devices Based on Interface-Engineered Field-Effect Transistor Biosensors Incorporated With Electronic Circuits. *Adv. Mater.* **2022**, *34*, No. 2203224.
(23) Yoon, J.; Conley, B. M.; Shin, M.; Choi, J.-H.; Bektas, C. K.; Choi, J.-W.; Lee, K.-B. Ultrasensitive Electrochemical Detection of Mutated Viral RNAs with Single-Nucleotide Resolution Using a Nanoporous Electrode Array (NPEA). *ACS Nano* **2022**, *16*, 5764−5777.
(24) Xiao, Y.; Lou, X.; Uzawa, T.; Plakos, K. J. I.; Plaxco, K. W.; Soh, H. T. An Electrochemical Sensor for Single Nucleotide Polymorphism Detection in Serum Based on a Triple-Stem DNA Probe. *J. Am. Chem. Soc.* **2009**, *131*, 15311−15316.
(25) Lai, W.; Ren, L.; Tang, Q.; Qu, X.; Li, J.; Wang, L.; Li, L.; Fan, C.; Pei, H. Programming Chemical Reaction Networks Using Intramolecular Conformational Motions of DNA. *ACS Nano* **2018**, *12*, 7093−7099.
(26) Huang, P.-J. J.; Liu, J. A DNA Aptamer for Theophylline with Ultrahigh Selectivity Reminiscent of the Classic RNA Aptamer. *ACS Chem. Biol.* **2022**, *17*, 2121−2129.
(27) Sun, C.; Xie, C.; Bu, G.-L.; Zhong, L.-Y.; Zeng, M.-S. Molecular Characteristics, Immune Evasion, and Impact of SARS-CoV-2 Variants. *Signal Transduct. Target. Ther.* **2022**, *7*, 202.
(28) Welch, N. L.; Zhu, M.; Hua, C.; Weller, J.; Mirhashemi, M. E.; Nguyen, T. G.; Mantena, S.; Bauer, M. R.; Shaw, B. M.; Ackerman, C. M.; et al. Multiplexed CRISPR-Based Microfluidic Platform for Clinical Testing of Respiratory Viruses and Identification of SARS-CoV-2 Variants. *Nat. Med.* **2022**, *28*, 1083−1094.
(29) Yang, Y.; Yang, X.; Zou, X.; Wu, S.; Wan, D.; Cao, A.; Liao, L.; Yuan, Q.; Duan, X. Ultrafine Graphene Nanomesh with Large On/Off Ratio for High-Performance Flexible Biosensors. *Adv. Funct. Mater.* **2017**, *27*, No. 1604096.
(30) Li, F.; Mao, X.; Li, F.; Li, M.; Shen, J.; Ge, Z.; Fan, C.; Zuo, X. Ultrafast DNA Sensors with DNA Framework-Bridged Hybridization Reactions. *J. Am. Chem. Soc.* **2020**, *142*, 9975−9981.
(31) Guo, J.; Shen, R.; Shen, X.; Zeng, B.; Yang, N.; Liang, H.; Yang, Y.; Yuan, Q. Construction of High Stability Indium Gallium Zinc Oxide Transistor Biosensors for Reliable Detection of Bladder Cancer-Associated MicroRNA. *Chin. Chem. Lett.* **2022**, *33*, 979−982.
(32) Ji, D.; Guo, M.; Wu, Y.; Liu, W.; Luo, S.; Wang, X.; Kang, H.; Chen, Y.; Dai, C.; Kong, D.; et al. Electrochemical Detection of a Few Copies of Unamplified SARS-CoV-2 Nucleic Acids by a Self-Actuated Molecular System. *J. Am. Chem. Soc.* **2022**, *144*, 13526−13537.
(33) Liu, J.; Chen, X.; Wang, Q.; Xiao, M.; Zhong, D.; Sun, W.; Zhang, G.; Zhang, Z. Ultrasensitive Monolayer MoS2 Field-Effect Transistor Based DNA Sensors for Screening of Down Syndrome. *Nano Lett.* **2019**, *19*, 1437−1444.
(34) Li, Y.; Zeng, B.; Yang, Y.; Liang, H.; Yang, Y.; Yuan, Q. Design of High Stability Thin-Film Transistor Biosensor for the Diagnosis of Bladder Cancer. *Chin. Chem. Lett.* **2020**, *31*, 1387−1391.
(35) Koklu, A.; Wustoni, S.; Guo, K.; Silva, R.; Salvigni, L.; Hama, A.; Diaz-Galicia, E.; Moser, M.; Marks, A.; McCulloch, I.; et al. Convection Driven Ultrarapid Protein Detection via Nanobody-Functionalized Organic Electrochemical Transistors. *Adv. Mater.* **2022**, *34*, No. 2202972.
(36) Guo, K.; Wustoni, S.; Koklu, A.; Díaz-Galicia, E.; Moser, M.; Hama, A.; Alqahtani, A. A.; Ahmad, A. N.; Alhamlan, F. S.; Shuaib, M.; Pain, A.; et al. Rapid Single-Molecule Detection of COVID-19 and MERS Antigens via Nanobody-Functionalized Organic Electrochemical Transistors. *Nat. Biomed. Eng.* **2021**, *5*, 666−677.
(37) Fung, T. S.; Liu, D. X. Similarities and Dissimilarities of COVID-19 and Other Coronavirus Diseases. *Annu. Rev. Microbiol.* **2021**, *75*, 19−47.
(38) Hoffmann, M.; Hofmann-Winkler, H.; Krüger, N.; Kempf, A.; Nehlmeier, I.; Graichen, L.; Arora, P.; Sidarovich, A.; Moldenhauer, A.-S.; Winkler, M. S.; et al. SARS-CoV-2 Variant B.1.617 is Resistant to Bamlanivimab and Evades Antibodies Induced by Infection and Vaccination. *Cell Rep.* **2021**, *36*, No. 109415.

(39) Garcia-Beltran, W. F.; Lam, E. C.; St. Denis, K.; Nitido, A. D.; Garcia, Z. H.; Hauser, B. M.; Feldman, J.; Pavlovic, M. N.; Gregory, D. J.; Poznansky, M. C.; et al. Multiple SARS-CoV-2 Variants Escape Neutralization by Vaccine-Induced Humoral Immunity. *Cell* **2021**, *184*, 2372−2383.e9.
(40) Wang, Y.; Yan, A.; Song, D.; Dong, C.; Rao, M.; Gao, Y.; Qi, R.; Ma, X.; Wang, Q.; Xu, H.; et al. Biparatopic Antibody BA7208/7125 Effectively Neutralizes SARS-CoV-2 Variants Including Omicron BA.1-BA.5. *Cell Discov.* **2023**, *9*, 3.

https://doi.org/10.1021/acssensors.3c00453
ACS Sens. 2023, 8, 2096−2104